International Journal for Numerical Methods in Fluids
Int. J. Numer. Meth. Fluids **26**: 235–247 (1998)

A SOLUTION-ADAPTIVE MESH PROCEDURE FOR PREDICTING CONFINED EXPLOSIONS

JOHN K. WATTERSON[a,*], ISOBEL J. CONNELL[b], A. MARK SAVILL[b] AND WILLIAM N. DAWES[b]

[a] *Department of Aeronautical Engineering, The Queen's University of Belfast, Belfast, UK*
[b] *Department of Engineering, University of Cambridge, Cambridge, UK*

SUMMARY

Explosion hazards constitute a significant practical problem for industry. In response to the need for better-resolved predictions for confined explosions, and particularly with a view to advancing safety cases for offshore oil and gas rigs, an existing unstructured, adaptive mesh, finite volume Reynolds-averaged Navier–Stokes computational fluid dynamics code (originally developed to handle non-combusting turbomachinery flows) has been modified to include a one-equation, eddy break-up combustion model. Two benefits accrue from the use of unstructured, solution-adaptive meshes: first, great geometrical flexibility is possible; second, automatic mesh adaptation allows computational effort to be focused on important or interesting areas of the flow by enhancing mesh resolution only where it is required. In the work reported here, the mesh was adaptively refined to achieve flame front capture, and it is shown that this results in a 10%–33% CPU saving for two-dimensional calculations and a saving of between 57% and 70% for three-dimensional calculations. The geometry of the three-dimensional calculations was relatively simple, and it may be expected that the use of unstructured meshes for truly complex geometries will result in CPU savings sufficient to allow an order-of-magnitude increase in either complexity or resolution. © 1998 John Wiley & Sons, Ltd.

KEY WORDS: confined explosions; risk assessment; CFD; adaptive mesh refinement; multiple obstacles

1. INTRODUCTION

It is widely recognized that the ability to predict accurately the types of combusting flows that may be encountered in the oil and gas production offshore environment is necessary in order to assess potential hazards and to design safety cases. This need was brought tragically to public notice by the Piper Alpha North Sea oil platform disaster in 1988. However, combustion leading to deflagration and possibly transition to detonation is itself a topic rich in complexity, as may be illustrated by the simple case of turbulent premixed flames in which the inherent problems of chemistry and thermodynamics are coupled in a non-linear manner with that of turbulence.

Substantial advances in understanding turbulent flames have been achieved through both experimental and numerical studies. In particular, model descriptions of turbulent flames based

* Correspondence to: Department of Aeronautical Engineering, The Queen's University of Belfast, Belfast, UK.

Contract grant sponsor: Shell Research Ltd.
Contract grant sponsor: EPSRC ROPA; Contract grant number: GR/K62324

CCC 0271–2091/98/020235–13$17.50

Received October 1996
Accepted April 1997

on experimental observations have been employed and tested in numerical studies, and it is now acknowledged that computational fluid dynamics (CFD) does have a role to play in the process of assessing risk and designing safer working environments. Indeed, a number of academic and commercial codes have been developed or adapted specifically to address this task. However, in the case of environments such as those which are typical of offshore oil and gas modules, the difficulty of adequately modelling turbulent flames is compounded by the geometric complexity of the flow domain. Flame propagation is critically dependent on the interaction between the flame chemistry and turbulence generated by obstacles in the flow, so accurate CFD predictions of a premixed explosion require adequate resolution of the turbulence generated by the flow. This is far from trivial. The ordinary difficulties of defining the geometry, generating a mesh, solving and postprocessing the solution, together with limitations of computer memory and speed, are magnified by the hundreds, even thousands, of obstacles that comprise a real rig, and then compounded by the need for adequate spatial resolution and turbulence modelling. Consequently, the ability to predict with consistent accuracy the overpressures generated by premixed explosions in the far more complex confined geometries, encountered for example in offshore modules, remains somewhat elusive.

A successful, if pragmatic, solution to this problem has been found by adapting the method of porosities and distributed resistances (PDR) [1,2], where realistic geometries are handled by resolving only the largest individual obstacles, while other 'subgrid-scale' obstacles (the majority) are modelled solely in terms of the volume they obstruct and as sources of drag and turbulence in the flow field. Resolved computations, e.g. Reference [3], using more refined combustion and turbulence models, have so far been confined to rather simplified model geometries containing typically up to 10 obstacles.

The work described in this paper falls somewhere between these two methods. A shock-capturing, unstructured, adaptive mesh Reynolds-averaged Navier–Stokes solver has been extended to handle transient flame fronts by the inclusion of a combustion model. The use of unstructured meshes allows much more complex geometries (in theory, several hundred obstacles) to be handled using existing computer resources, while mesh adaptation can be used to improve the solution resolution around obstacles and in their wakes, particularly as the flame front passes these. At present the method uses the k–ε turbulence model and a one-equation eddy break-up combustion method [4,5]; however, some limitations to these have already been identified, so work is already in progress to implement more sophisticated turbulence and combustion models.

2. NUMERICAL METHOD: FLOW SOLVER

The numerical method used in this study is the unstructured tetrahedral mesh method of Dawes [6–10] called un_NEWT. The method has been successfully used in a large number of turbomachinery flows, including: heat transfer in the serpentine coolant passage of a turbine blade and interaction between the coolant gas and the primary flow [6]; unsteady rotor–stator interaction [7]; and to aid interpretation of measured profile losses in unsteady turbine flows [8].

The latest version of the flow solver is time-accurate and includes a facility for solution-adaptive mesh refinement and coarsening which can be performed 'on the fly' in both space and time [9]. This means that when an unsteady flow feature such as a flame front or a wake passes through the computational domain, increased mesh resolution can be focused efficiently on the moving area of interest, while subsequent de-refinement ensures that the mesh automatically becomes coarse again when fine resolution is no longer required.

The equations solved are the fully three-dimensional, unsteady, Reynolds-averaged Navier–Stokes equations expressed in strong conservation form. Turbulence closure is provided by the $k-\varepsilon$ model together with a modified low-Reynolds-number model to handle the near-wall regions [10] and transition [11]. The seven equations of motion are cast in the absolute frame and are solved using the finite volume method of Jameson and Baker [12]. The primary control volumes are tetrahedral cells, and variables are stored at cell vertices. Assuming a piecewise linear variation of variables over the faces of the cells, a second-order-accurate discretization of the convective flux terms is achieved. The viscous stresses are calculated for each cell and are assumed to be piecewise constant over cells. The viscous fluxes can then be estimated for the nodes of the mesh using Gauss's divergence theorem. Artificial dissipation is added to control shock capture and solution decoupling. The smoothing consists of a blend of second- and fourth-order derivatives; the fourth-order terms operate throughout the solution domain and the second-order terms are adaptively switched on only in the presence of high pressure gradients. The net flux imbalance into each cell is used to update the flow field variables at the nodes, using four-stage Runge–Kutta time integration. Maximum local time steps may be used to enhance convergence of the solution procedure when steady state solutions are sought.

3. MESH GENERATION

Provided that the output file is correctly configured, any three-dimensional tetrahedral mesh generator can supply the mesh for the flow solver. Two meshing methods have been used in the current work. The first method employs a simple H-mesh generator to create a baseline structured mesh of hexahedra. Cell deletion may be used to generate new obstacles, e.g. a tube baffle may be created by deleting a row of cells. Each remaining hexahedron is then divided into six tetrahedra to form the unstructured mesh. This mesh retains the appearance of structure but does not inhibit the mesh refinement process. The second method used a Delaunay-type mesh generator. At the time of performing this work, only a two-dimensional version of the mesher was available, and three-dimensional meshes were developed by extruding the two-dimensional mesh regularly in the third dimension, which allowed some three-dimensional calculations to be performed.

4. MODELLING

4.1. Combustion model

At this stage the simplest possible combustion modelling has been employed. Details of the model may be found in References [13] and [14]. The model assumes that combustion is confined to a thin wrinkled flamelet region and that it may be described by a global, one-step, irreversible chemical reaction. A single progress variable, $\tilde{c}$, may then be introduced to describe the reaction interface and the zones of reactants and products. This variable might be, for example, a non-dimensional mass fraction of products of reaction, and its value would range from $\tilde{c}=0$ (in the reactants) to $\tilde{c}=1$ (in the products). A transport equation for the progress variable can then be written as

$$\frac{\partial}{\partial t}(\bar{\rho}\tilde{c})+\frac{\partial}{\partial x_k}(\bar{\rho}\tilde{c}\tilde{u}_k+\overline{\rho c'' u_k''})=\bar{w},$$

where $\overline{(\ )}$ denotes a Reynolds average, $\tilde{(\ )}$ denotes a Favre average and the Reynolds flux term $\rho c'' u_k''$ is modelled by a Bousinesq-type assumption:

$$\overline{\rho c'' u_k''} = -\mu_T \frac{\partial \tilde{c}}{\partial x_k}$$

Here μ_T is the turbulent viscosity and a Schmitt number of unity has been assumed. The source term $\bar{w}$ is described by an eddy break-up model as

$$\bar{w} = K\tilde{c}(1-\tilde{c})\bar{\rho}\frac{\tilde{\varepsilon}}{\tilde{k}}$$

where K is the EBU reaction rate constant, of order unity. The specific enthalpy is related to the temperature $\tilde{T}$ and the progress variable by

$$\tilde{h} = c_p \tilde{T} - \Delta\tilde{c}$$

where the heat release per unit mass of mixture, Δ, is related to the heat release parameter $\tau \equiv T_p/T_r - 1$ (where T_p and T_r are the product and reactant temperatures respectively), such that

$$\Delta = c_p T_r \tau$$

Values of K and τ can be obtained, given a knowledge of local strain, pressure, temperature, stoichiometry, etc., from suitable flamelet libraries. However, for the purposes of this work, values of $K = 3$ and $\tau = 5$ were taken as constants representative of the combustion of a stoichiometric methane–air mixture.

A characteristic of the EBU model is that very small values of $\tilde{c}$ can generate large but spurious source terms in regions of the flow where the ratio of dissipation rate to turbulent kinetic energy is large. This can lead to spurious ignition ahead of the flame owing to the transport of very small values of $\tilde{c}$. To counter this effect, leading edge suppression of the flame is implemented at the end of each time step. This is achieved by resetting the progress variable to zero at every node where its value falls below a cut-off value (chosen as 0.001). It was found that without leading edge suppression an incorrect flame shape was predicted for the HSE test case described below, with rapid progression of the flame front along the viscous boundaries and premature ignition close to the baffles owing to the high ratio $\tilde{\varepsilon}/\tilde{k}$ generated by the vortices in these regions.

4.2. Turbulence model

The precise low-Reynolds-number formulation adopted has been described in Reference [10]. It takes the form of a modified Lam and Bremhorst scheme [15], but with the damping function f_μ taken from the similar low-Reynolds-number model of Reynolds, and with y-dependence of the damping functions replaced by a dependence only on the turbulence Reynolds number [16]. This model has been shown to be adequate to model a wide variety of turbulence phenomena encountered in complex turbomachinery flows and has also been shown recently to capture boundary layer transition in the presence of mainstream turbulence [11]. However, it is not necessarily the optimum approach for modelling flow and combustion through arrays of obstacles, so work on the implementation of a more appropriate strain-dependent low-Reynolds-number model is currently under way [17].

4.3. Initial and boundary conditions

In common with many density-based methods, convergence difficulties occur with the flow solver at low Mach numbers, typically less than about 0.3. In the current work this was found to be especially acute during the laminar flame propagation phase of the calculations, particularly if the boundary at which ignition occurred was treated as closed. To maintain better flame shape during the initial propagation phase, it was found to be necessary to treat the ignition boundary as an inflow. The inflow boundary conditions specify the cold fluid total temperature and an inflow velocity. Specifying the total temperature for the cold fluid is equivalent to setting a positive constant value for the inflow total internal energy. Using the inflow velocity as the other condition avoids the need to set the total pressure at the boundary. Very small values of inlet velocity can be used, which are sufficiently small compared with the laminar burning velocity so as not to distort the flow development due to the combustion. $\tilde{k}$ and $\tilde{\varepsilon}$ are also defined at the inflow boundary. The values were chosen to produce vigorous flame propagation during the ignition process.

The ignition process is simulated by ramping the process variable from zero to one in the ignition region over a given period, i.e. a number of time steps. Since this is crude, it is important that the ramp is not too rapid, as this can result in the flame and flow developing out of phase and consequent flame extinction.

5. CALCULATIONS

The combustion version of the code has been applied to two sets of test cases. The first is two-dimensional, while the second generates a three-dimensional flow.

5.1. HSE test case

The first case is the baffled channel tests for which data have been supplied by the Health and Safety Executive (Buxton) Explosion and Flame Laboratory (hereafter referred to as HSE) [18]. The experimental configuration comprised a straight duct 1.2 m long with a square cross-section of width 0.3 m, within which uniformly spaced pairs of baffles (10 mm thick) were mounted symmetrically. Parametric studies were conducted in each of which the duct was filled with a stoichiometric mixture of fuel and air which was ignited at the closed end of the duct. The explosion vented into a large hanger. High-speed video was used to record the flame structure of the combusting flow, and pressures were recorded at points midway between the baffles.

This case may be considered as very nearly a two-dimensional flow and was treated as such. The HSE duct and a large volume beyond the duct vent were combined to form the computational domain (Figure 1). The H-mesh method was used to generate the initial meshes, and three cases were considered: five baffle pairs 75 mm tall; three baffle pairs 75 mm tall; and three baffle pairs 25 mm tall. Mesh refinement/de-refinement was performed every 50 time steps, and only one level of refinement was used. The criterion for refinement was that the local value of the progress variable be between 0.3 and 0.8. A uniform time step of 3.75 μs was used, and in Figure 1 the results are shown (for the case of five tall baffles) at intervals of 300 time steps, i.e. approximately every 1.12 ms. Planar ignition across the back wall of the baffled tube was assumed.

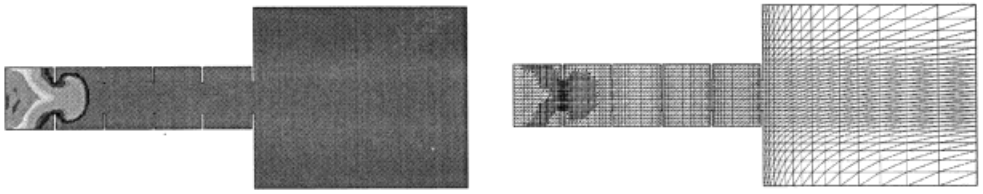

(a) Time = 1.12 ms

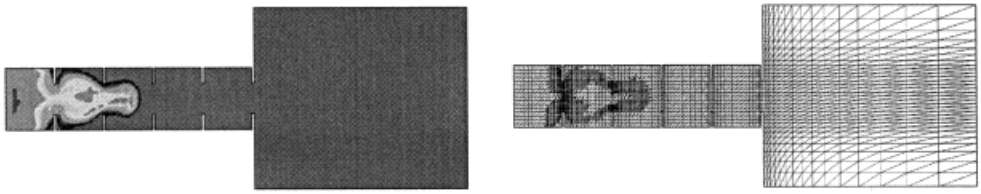

(b) Time = 2.25 ms

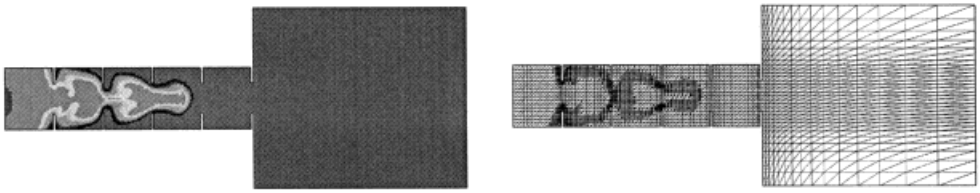

(c) Time = 3.38 ms

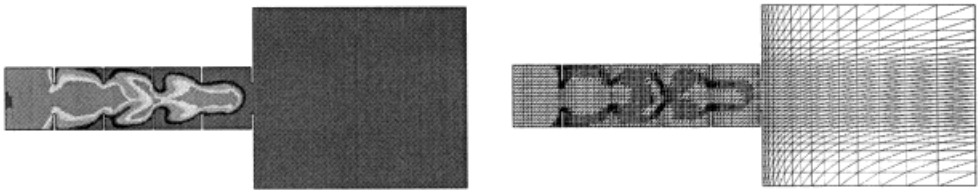

(d) Time = 4.50 ms

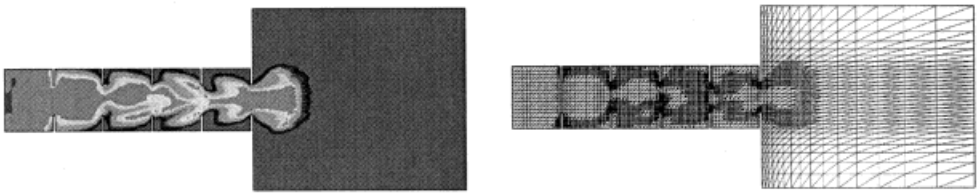

(e) Time = 5.62 ms

Figure 1. HSE test case: contours of progress variable and solution-adapted mesh

5.2. SOLVEX test case

The second test case employed was the internationally recognized SOLVEX (Shell Offshore Large Vented Explosion) box [19]. Designed by Shell Research to study experimentally the behaviour of confined, vented gas explosions at realistically large scales, the test facility comprised a 'box' with internal dimensions 10 m long by 8.75 m wide by 6.25 m tall. Parts of the walls were insulated with a 100 mm thick lagging to prevent pressure oscillations. It contained 14 cylindrical obstacles 0.5 m in diameter spanning the entire height of the box. The cylinders were placed in two rows of seven each which could be aligned or staggered and could be moved variable distances from the back wall of the box. The box was filled with a fuel and air mixture of stoichiometry 1.1, and combustion was initiated at the centre of the back wall by point ignition. The explosion vented to the atmosphere through the opposite end of the box via a vent which occupied 50% of the area of the wall.

Although the SOLVEX geometry is virtually two-dimensional, it results in a truly three-dimensional flow. The computational domain was generated using the Delaunay method. The two rows of cylindrical obstacles were placed 3.5 and 6.75 m from the back wall of the box and were staggered by half a pitch with respect to one another. The computational domain extended around the explosion box with the external boundaries 11.5 m downstream of the box vent and 4.375 m to either side; the upper and lower boundries were conterminous with the floor and ceiling of the box. The vent was modelled as spanning from ceiling to floor (6.25 m), and the effect of vent height, actually 4.65 m, was neglected. Thus the snapshots of the solution and mesh in Figure 2 show only a fraction of the total computational domain.

Three different ignition regions were considered:

1. ignition along a 1 m wide strip extending from floor to ceiling
2. ignition along a 0.1 m wide strip extending from floor to ceiling
3. ignition in a 0.1 m square region in the centre of the back wall.

In each case, ignition was modelled as a ramping of the progress variable from zero to one in the first 20 time steps.

Mesh refinement/de-refinement was performed every 50 time steps, and only one level of refinement was used. The criterion for refinement was that the local value of the progress variable be between 0.25 and 0.75. A uniform time step of 12.5 μs was used, and snapshots of the solution are shown (for case (3)) in Figure 2 at intervals of 400 time steps or 5 ms.

6. DISCUSSION

6.1. Explosion modelling

Consider first the results shown in Figures 1 and 2. Results are given for the HSE case with five tall baffle pairs and for the SOLVEX ignition case (3), i.e. the small ignition area. The figures show both the developing flame (revealed by the progress variable) and the solution-adapted mesh in selected snapshots. Qualitatively, the shapes of the flame brushes are good. In the HSE case the deformation of the flame as it passes through the sets of baffles is similar to the deformation reported in Reference [18]. Velocity vectors (not shown) show that there is significant development of the flow ahead of the flame brush. This flow development primes the fuel–air mixture ahead of the flame with the turbulence which will accelerate the burning process.

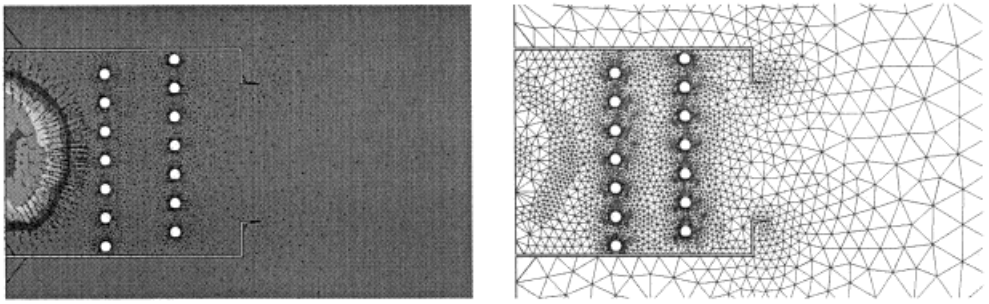

(a) Time = 5 ms

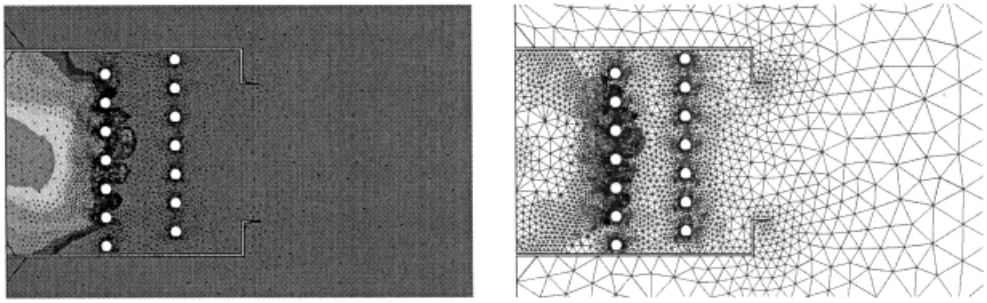

(b) Time = 10 ms

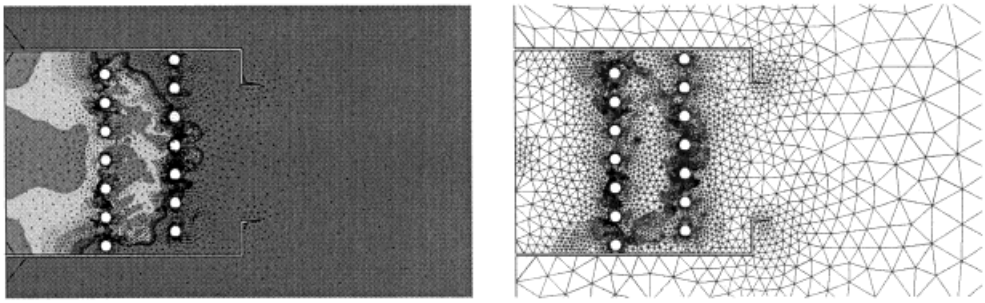

(c) Time = 15 ms

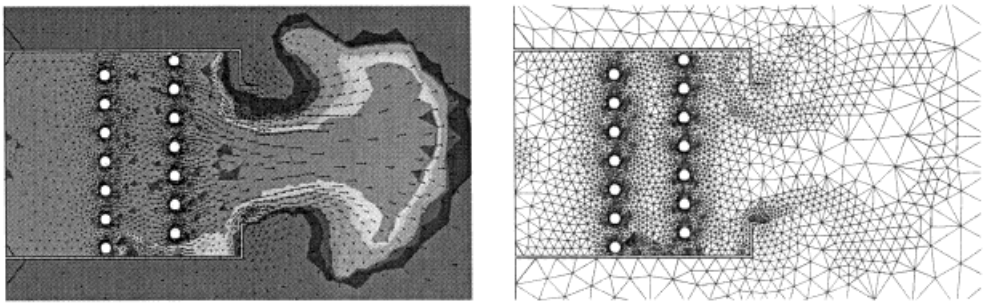

(d) Time = 20 ms

Figure 2. SOLVEX test case: contours of progress variable and solution-adapted mesh

Table I. Summary of HSE results

	Maximum overpressure (mbar)	Flame arrival time at first pair of baffles (ms)	Flame arrival time at baffles adjusted for laminar burning (ms)	Flame arrival time at vent (ms)	Flame arrival time at vent adjusted for laminar burning (ms)	Maximum flame speed at vent (m s^{-1})
Turbulent calculation	4500	1.0	121	5.5	125.5	220
Experiment	2000	65	—	100	—	170

Table II. Summary of SOLVEX results

	Maximum over pressure (mbar)	Time to maximum overpressure (ms)	Time to maximum overpressure adjusted for laminar burning (ms)	Maximum flame speed at vent (m s^{-1})
Turbulent calculation (1)	2670	30	905	110
Turbulent calculation (2)	1590	20	895	100
Turbulent calculation (3)	583	13	888	90
Experiment	180	907	—	66

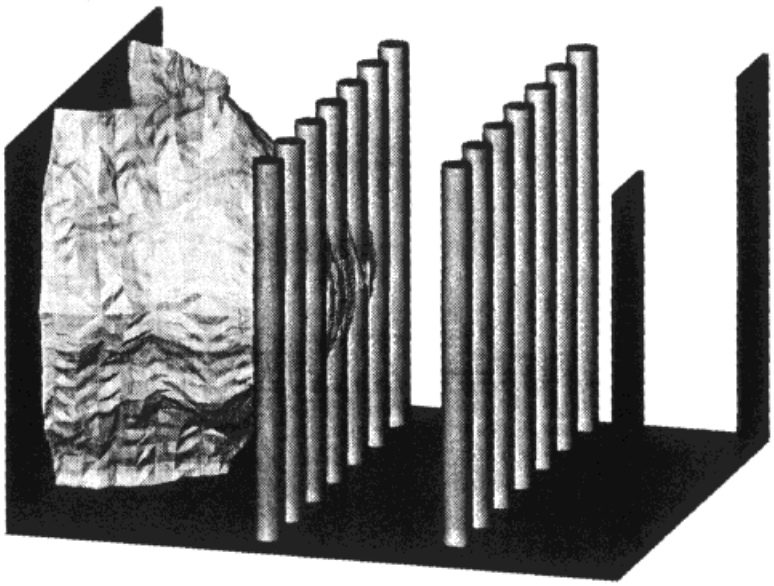

Figure 3. Perspective view of flame development in SOLVEX box: iso-surface for $\tilde{c} = 0.5$

Turning to the SOLVEX test case, it ought first to be noted that the results given in Figure 2 are for a plane slice through the midplane of the computational domain, and that in the third dimension the initial flame is spherical rather than cylindrical (Figure 3). Only limited information is available about the shape of the flame in the SOLVEX case, but it is in agreement with the predictions shown in Figure 2. The flame is roughly spherical (Figure 2(a)) until distorted by the first row of cylinders; this occurs at approximately a cylinder diameter in front of the first row. The flame can then be seen to start to fold (Figure 2(b)), the flame velocity between the obstacles increases with respect to the rest of the flame front, and fingering occurs. A similar process is observed as the flame passes through the second set of cylinders (Figure 2(c)); finally, there is a huge external explosion as the flame vents into the outer box, forming a large mushroom flame (Figure 2(d)).

A comparison between experimental and numerical results for the HSE case is given in Table I and for the SOLVEX case in Table II. In the HSE case the predicted peak overpressure is more than twice the measured value. The predicted maximum overpressure was obtained midway between the first pair of baffles shortly after ignition. Overpressures were also recorded along the centreline between the other pairs of baffles and on the lower wall between baffle pairs. All other peak overpressures were between 2.5 and 3.0 bar.

Table III. Comparison of mesh sizes for HSE test case

	No. of nodes	No. of cells
Initial mesh	5313	19320
Intermediate mesh	14214	69712
Uniformly refined mesh	21252	77280

Table IV. Comparison of mesh sizes for SOLVEX test case

	No. of nodes	No. of cells
Initial mesh	10221	38916
Intermediate mesh	25368	135280
Uniformly refined mesh	81768	311328

In the SOLVEX case (Table II) the overpressure is greatly overpredicted. Starting with case (1) with the largest ignition area, the predicted overpressure is more than one order of magnitude too large; for the smaller ignition strip (case (2)) the predicted overpressure is just under one order of magnitude too large; and for the smallest ignition area (case (3)) the predicted overpressure is a factor of 3.2 too large. Clearly the ignition area is an important parameter.

Comparison between predicted and measured flame arrival and peak overpressure times is very poor; generally speaking, the predicted values are about two orders of magnitude smaller than the measured values. As shown in Reference [5], this can be explained by the failure of the numerical method to model the laminar burning phase of the explosion. The laminar burning velocity for a stoichiometric methane–air mixture is about 0.5 m s^{-1}. With expansion ratios of four (two-dimensional HSE case) and eight (three-dimensional SOLVEX case), this leads to laminar flame speeds of 2 and 4 m s^{-1} respectively. In the HSE case then the time for arrival of the flame at the first pair of baffles (0.24 m from the ignition site) is about 120 ms, while in the SOLVEX case the time for flame arrival at the first set of cylinders (3.5 m from the ignition site) is about 875 ms. Since these figures are reassuringly close to the experimental results, it is expected that when proper laminar flame modelling is included, the predicted times will be much closer to the experimental values. It is also expected that the vigorous burning presently predicted is responsible for the excessive overpressures predicted even when the ignition site is reduced in area. It is hoped that laminar flame modelling will reduce the predicted overpressures to values closer to the experimental results.

6.2. Benefits of adaptive mesh refinement

One of the clear benefits of using unstructured meshes is the ability to produce a mesh for arbitrarily complex geometries. However, unstructured meshes also allow solution-adaptive mesh refinement/de-refinement, with the benefit that more efficient meshes become possible. It is instructive to attempt to quantify this benefit. Tables III and IV give the numbers of nodes and cells in the meshes used in the HSE and SOLVEX calculations respectively. Values are given for the initial, unadapted mesh, then for a representative intermediate adapted mesh and finally for a uniformly refined mesh based on doubling the resolution of the initial mesh.

The HSE calculation employed an initial mesh of 5313 nodes and 19 320 cells. Mesh refinement resulted in a mesh with approximately 2.7 times more nodes and 3.6 times more cells. Comparing the intermediate and uniformly refined meshes shows a saving of 33% on the nodes and 10% on the cells. These savings are not as large as might be expected, but can be explained as follows. Although the flow regime was assumed to be two-dimensional, the calculation used a three-dimensional mesh which was three nodes and four cells deep. Mesh refinement was three-dimensional, resulting in refined regions being five nodes and eight cells deep. However, the uniformly refined mesh is obtained by refining only in two rather than three dimensions, thus multiplying the initial mesh size by four rather than eight. The

implication is that a three-dimensional, unstructured flow solver is not used to its best efficiency when applied to two-dimensional calculations.

Turning to the three-dimensional SOLVEX calculation, summarized in Table IV, we see a different story. The intermediate mesh uses only 2.5 times as many nodes as the initial mesh but 3.5 times as many cells, a result similar to the HSE case. However, the comparison between the intermediate and uniformly refined meshes is much more favourable in this case. The saving on nodes is 70% and on cells is 57%. This is clearly because the uniformly refined mesh would require to be refined in all three dimensions, resulting in an eightfold increase on the initial mesh. These savings are significant and can be translated into increased resolution of obstacles or more complex geometries. Indeed, it is expected that the CPU savings will increase further for more complex geometries, bringing closer the use of the numerical method for truly complex geometries more representative of industrial structures.

7. CONCLUSIONS

A simple combustion model using the idea of a progress variable to describe the extent of burning has been implemented within an existing unstructured mesh CFD code and has been tested against two sets of experimental data. Substantial reductions of computational effort between 10% and 70% have been obtained through the use of solution-adaptive refinement and coarsening of the mesh. The greater savings are available for three-dimensional geometries, and these can be translated into increased resolution of obstacles or increased number of obstacles resolved. This points towards the eventual use of the unstructured mesh method for calculations of industrial complexity.

For both two- and three-dimensional flows the method has been shown to predict flow field and flame development in close agreement with experimental observations, implying that the effect of combustion on the fluid mechanics has been correctly captured. However, the predicted overpressures and times for flame arrival or times to peak overpressure are still wrong. The predicted overpressures are at most about four times larger than the measured values; the predicted flame arrival and peak overpressure times are approximately two orders of magnitude too small. It has been shown that modelling of the ignition process is probably responsible for much of this inaccuracy. Three areas for improvement have been identified.

1. Laminar flame propagation modelling is essential if the peak overpressures and characteristic times are to be better predicted. The ignition process also influences the initial flame propagation and requires careful modelling.
2. More sophisticated combustion modelling, e.g. dependence on a laminar flamelet library, will be required to properly capture the interaction between the fluid mechanics and the flame burning and the effect of different fuel–air mixtures.
3. Since the present version of the k–ε low-Reynolds-number model is not optimal for confined geometries, more sophisticated turbulence modelling will be necessary, e.g. more advanced k–ε and perhaps, later, Reynolds stress transport models.

Finally, it is hoped that it will be possible to move to application of this method to real modules using CAD interface and parallel computing plus the latest visualization software. The research reported in this paper is regarded as progress towards that goal.

ACKNOWLEDGEMENTS

This research has been funded by Shell Research Ltd. and by EPSRC ROPA grant GR/K62324. The help and encouragement of the staff at the Shell Research and Technology Centre Thornton are gratefully acknowledged, as is also the assistance of colleagues at HSE and Tel-Tek.

REFERENCES

1. B.H. Hjertäger, T. Solberg and K.O. Nymoen, 'Computer modelling of gas explosion propagation in offshore modules', *J. Loss Prevent. Process Ind.*, **5**, 165–173 (1992).
2. A.M. Savill and T. Solberg, 'Some improvements to PDR/$k-\varepsilon$ model predictions for explosions in confined geometries', *Proc. IMA/ERCOFTAC Conf. on Flow and Dispersion through Groups of Obstacles*, Cambridge, 1994.
3. P.S. Barsanti, K.N.C. Bray and R.S. Cant, 'Modelling of confined turbulent explosions', in R. Bower (ed.), *Combustion Science and Technology Book Series*, 1994.
4. J.K. Watterson, A.M. Savill, W.N. Dawes and K.N.C. Bray, 'Predicting confined explosions with an unstructured adaptive mesh code', *Joint Meet. of the Portuguese, British and Spanish Sections of the Combustion Institute*, Madeira, 1996.
5. I.J. Connell, J.K. Watterson, A.M. Savill, W.N. Dawes and K.N.C. Bray, 'An unstructured adaptive mesh CFD approach to predicting confined premixed methane–air explosions', *Second. Int. Specialist Meet. on Fuel–Air Explosions*, Bergen, 1996.
6. W.N. Dawes, 'The practical application of solution-adaption to the numerical solution of complex turbomachinery problems', *Prog. Aerospace Sci.*, **29**, 221–269 (1993).
7. W.N. Dawes, 'A numerical study of the interaction of a transonic compressor rotor overtip leakage vortex with the following stator blade row', *ASME–IGTI Conf.*, The Hague, 1994, Paper 94-GT-156.
8. H.P. Hodson and W.N. Dawes, 'On the interpretation of measured profile losses in unsteady wake–turbine blade interaction studies', *ASME–IGTI Conf.*, Birmingham, 1996.
9. W.N. Dawes, 'Simulating unsteady turbomachinery flows on unstructured meshes which adapt both in time and space', *ASME–IGTI Conf.*, 1993, Paper 93-GT-104.
10. W.N. Dawes, 'Development of a solution-adaptive 3D Navier–Stokes solver for turbomachinery', *AIAA/ASME/SAE/ASEE 27th Joint Propulsion Conf.*, 1991, Paper 91-2469-CP.
11. A.M. Savill, 'One-point closures applied to transition', in *Turbulence and Transition Modelling*, Kuiver, 1996, Chap. 6.
12. A. Jameson and T.J. Baker, 'Improvements to the aircraft Euler method', *AIAA Paper 87-045*, 1987.
13. K.N.C. Bray, P.A. Libby and J.B. Moss, 'Unified modelling approach for premixed turbulent combustion—Part 1: General formulation', *Combust. Flame*, **61**, 87–102 (1985).
14. P.S. Barsanti, 'Simulations of confined turbulent explosions', *Ph.D. Dissertation*, University of Cambridge, (1994).
15. C.K.G. Lam and K.A. Bremhorst, 'Modified form of the $k-\varepsilon$ model for predicting wall turbulence', *J. Fluids Engng.*, **103**, 456–460 (1981).
16. V.C. Patel, W. Rodi and G. Scheuerer, 'Turbulence models for near-wall flows and low Reynolds numbers: a review', *AIAA J.*, **23**, 1308–1319 (1985).
17. J.K. Watterson, W.N. Dawes, A.M. Savill and A.J. White, 'Turbulent flow in a staggered bundle of cylinders without heat transfer', *3rd ERCOFTAC–IAHR Workshop on Refined Flow Modelling*, Lisbon, 1994.
18. D.J. Freeman, 'Visualisation of explosions in a baffled plate, vented enclosure', *Health and Safety Executive Explosion and Flame Laboratory, Rep. IR/L/GE/94/08*, 1994.
19. J.S. Puttock, T.M. Cresswell, P.R. Marks, A. Samuels and A. Prothero, 'Explosion assessment in confined vented geometries. SOLVEX large scale explosion tests and SCOPE model development. Project report', *Shell Research Limited, Rep. TRCP 3688R2*, 1995.

